Raman Evidence for Specific Substrate-Induced Structural Changes in the Heme Pocket of Human Cytochrome P450 Aromatase during the Three Consecutive Oxygen Activation Steps†

Takehiko Tosha,‡ Norio Kagawa,§ Takehiro Ohta,‡,|| Shiro Yoshioka,§,⊥ Michael R. Waterman,§ and Teizo Kitagawa*,‡

Okazaki Institute for Integrative Bioscience, National Institutes of Natural Sciences, Okazaki 444-8787, Japan, and Department of Biochemistry, Vanderbilt University School of Medicine, Nashville, Tennessee 37232-0146

Received January 17, 2006; Revised Manuscript Received March 14, 2006

ABSTRACT: Specific substrate-induced structural changes in the heme pocket are proposed for human cytochrome P450 aromatase (P450arom) which undergoes three consecutive oxygen activation steps. We have experimentally investigated this heme environment by resonance Raman spectra of both substrate-free and substrate-bound forms of the purified enzyme. The Fe−CO stretching mode (ν_{Fe-CO}) of the CO complex and Fe^{3+}−S stretching mode (ν_{Fe-S}) of the oxidized form were monitored as a structural marker of the distal and proximal sides of the heme, respectively. The ν_{Fe-CO} mode was upshifted from 477 to 485 and to 490 cm^{-1} by the binding of androstenedione and 19-aldehyde-androstenedione, substrates for the first and third steps, respectively, whereas ν_{Fe-CO} was not observed for P450arom with 19-hydroxyandrostenedione, a substrate for the second step, indicating that the heme distal site is very flexible and changes its structure depending on the substrate. The 19-aldehyde-androstenedione binding could reduce the electron donation from the axial thiolate, which was evident from the low-frequency shift of ν_{Fe-S} by 5 cm^{-1} compared to that of androstenedione-bound P450arom. Changes in the environment in the heme distal site and the reduced electron donation from the axial thiolate upon 19-aldehyde-androstenedione binding might stabilize the ferric peroxo species, an active intermediate for the third step, with the suppression of the formation of compound I (Fe^{4+}═O porphyrin$^{+\bullet}$) that is the active species for the first and second steps. We, therefore, propose that the substrates can regulate the formation of alternative reaction intermediates by modulating the structure on both the heme distal and proximal sites in P450arom.

Cytochrome P450 aromatase (P450arom),[1] CYP19, catalyzes the final step for the biosynthesis of estrogens (*1*, *2*). The enzyme is widely distributed in gonads and extragonadal tissues, including ovary, testis, brain, skin, and adipose tissue for the regulation of hormone balance (*3*, *4*), and is related to several hormone-dependent diseases such as breast cancer (*5*−*7*). The P450arom-catalyzed reaction exhibits a complex nature consisting of three consecutive oxygen activation steps, converting C19 androgens such as androstenedione (AD) and testosterone (Test) to aromatic C18 estrogenic steroids (*1*, *2*, *8*−*10*) as shown in Figure 1. The first and second oxidative steps are hydroxylations at C19 of androgens by a ferryl porphyrin π-cation radical species, which corresponds to compound I of heme proteins including peroxidases and P450s (*11*, *12*). The third oxidative step cleaves the C10−C19 bond in the 19-aldehyde androgen, which is nonenzymatically produced by dehydration of 19-diol androgen, with the specific removal of the 1β and 2β hydrogens to aromatize the steroid A-ring and the release of formate (*2*, *9*, *10*). Several lines of studies on the mechanism for the third oxidative step propose that a ferric peroxo intermediate (Fe^{3+}−OO^{-}) but not compound I acts as an active species, and the nucleophilic attack of the ferric peroxo species on the carbonyl carbon of the aldehyde group triggers the third oxidative reaction (*2*, *9*, *10*, *13*, *14*).

Similar to the P450arom-catalyzed reactions, multiple reaction steps catalyzed by multiple reactive intermediates are reported for lanosterol 14α-demethylase (CYP51) (*15*), progesterone 17α-hydroxylase/17,20-lyase (CYP17) (*16*−*18*), and nitric oxide synthase (NOS) (*19*, *20*). In addition, compound I or ferric peroxo species possibly works as an alternative intermediate in several P450s (*21*, *22*). While the ferric peroxo species is now widely accepted as an additional

† This work was supported by Grant-in-Aid for Specifically Promoted Research (14001004 to T.K.) from the Ministry of Education, Culture, Sports, Science, and Technology, Japan, and NIH Grants GM37942 and ES00267. T.T. was supported by a research fellowship from the Japan Society for the Promotion of Science for young scientists.

* To whom correspondence should be addressed. Phone: +81-564-59-5225. Fax: +81-564-59-5229. E-mail: teizo@ims.ac.jp.

‡ National Institutes of Natural Sciences.

§ Vanderbilt University School of Medicine.

|| Present address: Department of Chemistry, Stanford University, Stanford, CA 94305.

⊥ Present address: Okazaki Institute for Integrative Bioscience, National Institutes of Natural Sciences, Okazaki 444-8787, Japan.

[1] Abbreviations: P450arom, cytochrome P450 aromatase; AD, androstenedione; Test, testosterone; 19-aldo-AD, 19-aldehyde-AD; 19-OH-AD, 19-hydroxy-AD; RR, resonance Raman; 6cLS, 6-coordinate/low spin; 5cHS, 5-coordinate/high spin; P450cam, cytochrome P450 camphor; NOS, nitric oxide synthase; CPO, chloroperoxidase; P450 BM3, cytochrome P450 from *Bacillus megaterium*.

10.1021/bi060094a CCC: $33.50
Published on Web 04/07/2006

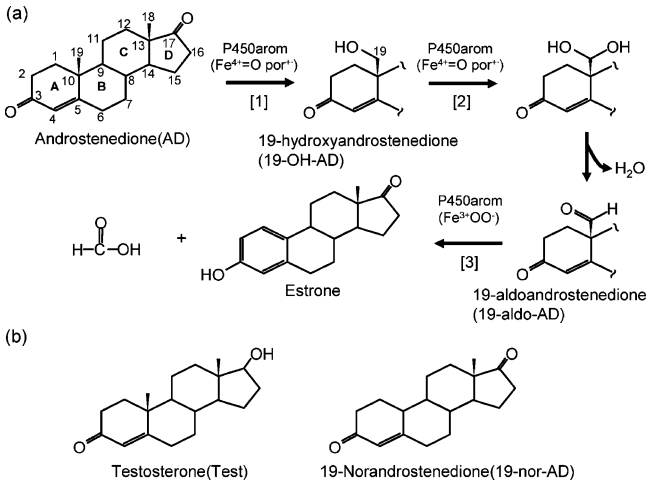

FIGURE 1: Proposed reaction mechanism for the aromatization of androstenedione by P450arom (a) and the chemical structures of a substrate and analogue used in this study (b). While a ferryl oxo porphyrin π cation radical (Fe^{4+}═O porphyrin$^{+\bullet}$), compound I, is supposed to be an active species for the first and second steps ([1] and [2]) in the aromatization reaction, the ferric peroxo species ($Fe^{3+}OO^{-}$) is proposed to act as the active species in the final step ([3]).

reaction intermediate in the P450 chemistry (*23*), the regulation mechanism for the formation of alternative reaction intermediates has been poorly understood.

To interpret the mechanism for the three consecutive oxygen activation steps in P450arom, Graham-Lorence et al. constructed the structural model for P450arom (*24*). They proposed that the 19-aldehyde androgen could induce the rearrangement of the conserved distal Thr, which is crucial for the formation of compound I, through a hydrogen-bonding interaction. Such displacement of the distal Thr could suppress the formation of compound I and stabilize the ferric peroxo species only in the third oxidative step (*24*). However, there is no structural evidence that the substrate modulates the distal heme environment for formation of the alternative reaction intermediates in P450arom. It is still unclear how P450arom regulates the formation of the alternative intermediates for the successive multiple oxidative steps mainly due to the lack of structural information on the heme active site in P450arom.

Although it is desirable to characterize the structure of the heme active site in P450arom for understanding the mechanism of the formation of alternative intermediates, so far, the difficulty in obtaining high-quality samples has hampered spectroscopic characterization of P450arom. Recently, Kagawa et al. developed an *Escherichia coli* expression system of human P450arom and purified it as a stable form (*25*, *26*), allowing us to examine the heme active site structure by utilizing spectroscopic techniques.

In this study, we applied resonance Raman (RR) spectroscopy to structural characterization of human P450arom. RR spectroscopy is a powerful tool to explore the heme environment in the solution state and requires a moderate amount of sample (e.g., 100 μL of 50 μM solutions). Besides the porphyrin skeletal vibrations, which reflect the coordination structure and spin state of the heme (*27*, *28*), the CO-associated vibrations in the CO adduct are useful to characterize the environment of the heme distal site and the property of an axial ligand (*29*−*31*). Furthermore, the iron−axial ligand stretching mode (ν_{Fe-S}) should serve as a structural marker at the heme proximal site. We found that the environments of both heme distal and proximal sides depend on the substrates by comparing the Raman lines for substrate-free with those of the substrate-bound forms of P450arom, where substrates include AD, Test, 19-hydroxy-AD (19-OH-AD), and 19-aldehyde-AD (19-aldo-AD) and an analogue (19-nor-AD), in which C19 is absent (Figure 1b). Because the distal environment and the strength of the Fe−S bond could be essential for the formation of a specific reaction intermediate (*32*), the finding in this study should produce new insights into the multiple oxidative reactions by P450s such as P450arom.

MATERIALS AND METHODS

Materials. Substrates 19-OH-AD and 19-aldo-AD were purchased from Steraloids. The solution of 45% (w/v) 2-hydroxypropyl-β-cyclodextrin in water was obtained from Sigma. Isotopically labeled CO, $^{13}C^{18}O$, was acquired from Cambridge Isotope Laboratories, Inc. (Andover, MA). All other reagents with highest purity were purchased from Wako (Osaka, Japan) and Nacalai tesque (Kyoto, Japan).

Expression and Purification of P450arom. Human P450arom is found to be polymorphic at residue 264 (Arg/Cys) (*33*). Both forms were expressed as functional P450arom but the Arg form is more stable (*25*, *26*) and is used in subsequent studies. The *E. coli* expression and purification of P450arom were carried out as described (*25*, *26*). The purified substrate-free P450arom in 100 mM sodium phosphate buffer, pH 7.4, containing 20% glycerol, 1% Tween 20, 1% sodium cholate, 0.1 mM EDTA, and 0.1 mM DTT, was stored at −80 °C.

Optical Spectroscopy. UV/vis absorption spectra were recorded on a U-3310 spectrometer (Hitachi). Each substrate was dissolved in 45% (w/v) 2-hydroxypropyl-β-cyclodextrin in water and stored as a 50 mM stock solution at 4 °C. Substrates (10 μL of the stock solution) were added to 490 μL of substrate-free P450arom (10 μM) to generate substrate-bound forms. The ferrous−CO form of P450arom was produced by the addition of 1 μL of the dithionite solution (∼100 mM) under CO atmosphere.

Resonance Raman Spectroscopy. RR spectra were obtained with a single polychromater (Jobin Yvon, SPEX750M) equipped with a liquid nitrogen-cooled CCD detector (Roper Scientific, Spec 10:400B/LN). The 406.7 nm line from a Kr^{+} laser (Spectra Physics, BeamLok 2060) and the 441.6 nm line from a He−Cd laser (Kinmon Electric, model CD4805R) were used for the excitation of ferric and ferrous−CO forms of P450arom, respectively. To observe the Fe^{3+}−S stretching mode (ν_{Fe-S}), the 363.8 nm line from an Ar^{+} laser (Spectra Physics, BeamLok 2080) was used as the excitation source. The laser power was adjusted to 1−2 mW at the sample point. Raman shifts were calibrated with indene, acetone, and carbon tetrachloride. All measurements were performed at ∼4 °C with a spinning cell (2000 rpm) for sample concentrations of 30−60 μM.

RESULTS

UV/vis Absorption Spectra of Ferric P450arom. To characterize the heme environment of P450arom with and without a substrate, we measured the UV/vis absorption

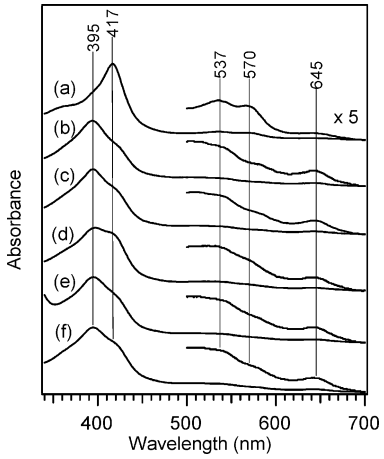

FIGURE 2: Optical absorption spectra of ferric P450arom in the absence (a) and presence of AD (b), Test (c), 19-OH-AD (d), 19-aldo-AD (e), and 19-nor-AD (f).

spectra. UV/vis absorption spectra for ferric forms of substrate-free P450arom and AD-, Test-, 19-OH-AD-, and 19-aldo-AD-bound P450arom are shown in Figure 2. As previously reported (*25*), substrate-free P450arom exhibits a Soret maximum at 417 nm, an α-band at 570 nm, and a *β*-band at 537 nm, indicating that the heme iron in substrate-free P450arom is in a 6-coordinate/low-spin (6cLS) state. The binding of substrates, AD, Test, and 19-aldo-AD, showed the transition of the coordination structure and the spin state of the heme iron to a 5-coordinate/high-spin (5cHS) state, which is evident from the blue shift of the Soret peak to ∼395 nm and the appearance of a charge-transfer band at 645 nm (*34*). This structural transition of the heme is due to the dissociation of the sixth ligand such as a water molecule upon the binding of the substrates.

Contrary to the other substrate-bound forms of P450arom, the 19-OH-AD-bound enzyme exhibits a mixture of the 6cLS and 5cHS states (Figure 2d). Further addition of 19-OH-AD to P450arom showed no further spectral change (data not shown), indicating that the remaining 6cLS state did not arise from the substrate-free enzyme. It is, therefore, likely that in the 6cLS form the 19-hydroxyl group might stabilize a water ligand at the sixth coordination position through a hydrogen bond or that the 19-hydroxyl group might directly interact with the heme iron as the hydroxyl group of the product for P450cam weakly interacts with the heme iron (*35*).

We measured the UV/vis absorption spectrum of P450arom with 19-nor-AD, in which the C19 group is absent, to examine the role of the C19 group in the structural transition upon the binding of substrates. As shown in Figure 2f, the addition of 19-nor-AD also induced the formation of the 5cHS state. We can conclude that the C19 group is not crucial for the structural transition of the spin state and coordination structure in the heme upon substrate binding and suggest that the steroid ring could lie in close proximity to the heme iron.

Resonance Raman Spectra of Ferric P450arom. To obtain further insight into the structural environment of the heme of P450arom, we measured their RR spectra. Figure 3 displays RR spectra of ferric P450arom in the absence and presence of substrates and analogue with 406.7 nm excitation. In the high-frequency region of RR spectra (Figure 3A),

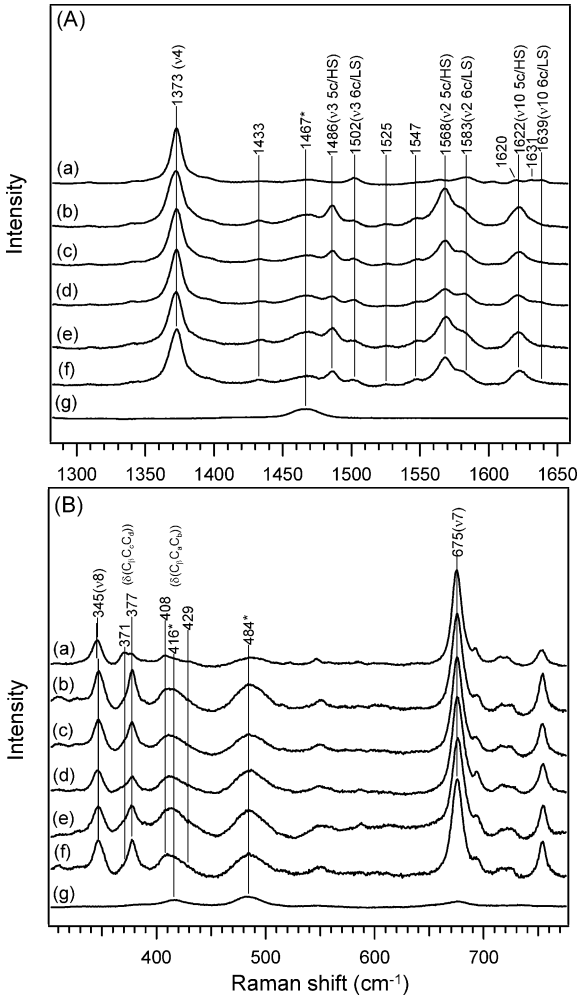

FIGURE 3: Resonance Raman spectra of ferric P450arom excited at 406.7 nm. Panels A and B represent the high- and low-frequency regions of the resonance Raman spectra, respectively. Traces shown were obtained from ferric P450arom in the absence of substrate (a) and in the presence of AD (b), Test (c), 19-OH-AD (d), 19-aldo-AD (e), and 19-nor-AD (f) and the spectrum of buffer used in this measurement (g). The Raman lines from glycerol in the buffer are denoted by an asterisk. The laser power was 1.5 mW at the sample point.

several porphyrin marker lines, ν_4, ν_3, ν_2, and ν_{10}, are useful to characterize the heme active site structure (*27*, *28*). For the substrate-free P450arom [Figure 3A(a)], the oxidation state marker, ν_4, appears at 1373 cm^{-1}. The core size markers, ν_3 and ν_2, which are sensitive to the spin and coordination states of the heme iron, are observed at 1502 and 1583 cm^{-1}, respectively. We assigned the Raman line at 1639 cm^{-1} to the ν_{10} vibration from its depolarized character in the polarization experiment (data not shown). The ν_4, ν_3, ν_2, and ν_{10} vibrations at 1373, 1502, 1583, and 1639 cm^{-1}, respectively, are characteristic of the 6cLS heme. Consistent with the optical spectrum, these frequencies are indicative of the 6cLS state in the heme iron for substrate-free P450arom.

Although the Raman lines arising from the 6cLS heme were still detected as a minor component, the Raman lines at 1486, 1568, and 1622 cm^{-1} assignable to the ν_3, ν_2, and ν_{10} vibrations of the 5cHS heme, respectively, were predominant for the substrate- and analogue-bound forms of P450arom [Figure 3A(b−f)]. In 19-OH-AD-bound P450arom, the fraction of the 6cLS heme was relatively large, as

Table 1: Frequencies (cm^{-1}) of the Heme Marker Lines for P450arom and Other Thiolate-Ligated Enzymes

sample	ν_4	ν_3	ν_2	ν_{10}	state	ref
P450arom	1373	1502	1583	1639	6cLS	this study
+AD	1369[a]	1486	1568	1622	5cHS	this study
+Test	1369[a]	1486	1568	1622	5cHS	this study
+19-OH-AD	1369[a]	1486	1568	1622	5cHS	this study
	1373	1502	1583	1639	6cLS	this study
+19-aldo-AD	1369[a]	1486	1568	1622	5cHS	this study
+19-nor-AD	1369[a]	1486	1568	1622	5cHS	this study
P450cam	1373	1503	1584	1635	6cLS	*34*
+D-camphor	1368	1488	1570	1623	5cHS	*34*
P450 BM3	1374	1502	1583	1638	6cLS	*46*
+arachidonic acid	1372	1487	1570	nd[b]	5cHS	*46*
MtCYP51[c]	1373	1504	1584	1638	6cLS	*62*
+2PhIm[d]	1372	1503	1583	1639	6cLS	*62*
	nd[b]	1488	nd[b]	nd[b]	5cHS	*62*
TXAS[e]	1373	1503	1584	1635	6cLS	*54*
+CTA_2[f]	1373	1503	1586	1638	6cLS	*54*
	1371	1487	1568	nd[b]	5cHS	*54*
eNOS[g]	1374	1503	1579	1635	6cLS	*48*
+L-Arg	1370	1489	1563	nd[b]	5cHS	*48*
CPO[h]	1374	1505	nd[b]	1640	6cLS	*63*
	1369	1490	1564	1627	5cHS	*64*

[a] The Raman line at 1373 cm^{-1} observed with 406.7 nm excitation (Figure 3) is probably due to the contribution from the 6cLS species. The ν_4 vibration for the 5cHS state was detected at 1369 cm^{-1} upon excitation at 363.8 nm (data not shown). Such observation was also reported in other P450s (*65*). [b] nd: not determined. [c] Sterol 14a-demethylase cytochrome P450 from *Mycobacterium tuberculosis*. [d] 2-Phenylimidazole. [e] Thromboxane synthase. [f] Carbocyclic thromboxane A_2. [g] Endothelial nitric oxide synthase. [h] Chloroperoxidase.

Table 2: Frequencies (cm^{-1}) of the Heme Skeletal and Peripheral Vibrations Observed in the Low-Frequency Region

sample	ν_8	$\delta(C_\beta C_c C_d)$	$\delta(C_\beta C_a C_b)$	ν_7
P450arom	345	371, 377	408, 429	675
+AD	346	377	~416[a]	676
+Test	346	377	~416[a]	676
+19-OH-AD	346	377	~416[a]	676
+19-aldo-AD	346	377	~416[a]	676
+19-nor-AD	346	377	~416[a]	676

[a] We cannot determine the specific peak position due to the overlapping with the Raman line from glycerol.

indicated from the optical spectrum. These assignments of Raman lines are summarized in Table 1 together with those of other P450s and NOSs.

In the low-frequency region (Figure 3B), we can detect the Raman lines arising from the vibrations including the heme peripheral groups as well as the porphyrin skeletal vibrations (*36*, *37*). Thus, the Raman lines observed in the low-frequency region can provide information on the interaction between the heme prosthetic group and protein environment. The intense Raman lines at 675 and 345 cm^{-1} in substrate-free P450arom can be assigned to ν_7 and ν_8, respectively [Figure 3B(a)]. By analogy to the Raman spectra of other heme proteins (*36*, *37*), the Raman lines at 371 and 377 cm^{-1} are assigned to the bending modes of the heme propionate groups, $\delta(C_\beta C_c C_d)$, and the Raman lines at 406 and 429 cm^{-1} can be assigned to the bending modes of the heme vinyl groups, $\delta(C_\beta C_a C_b)$. These assignments are summarized in Table 2.

As shown in Figure 3B, the binding of the substrates and analogue to P450arom results in the changes in the bending modes of the heme vinyl and propionate groups without noticeable changes in other Raman lines observed in this region. The peak position of the bending mode of the heme vinyl group cannot be determined due to the overlapping with the glycerol peak. The bending mode of the heme propionate at 371 cm^{-1} in substrate-free P450arom was missing while the peak at 377 cm^{-1} remains upon the addition of the substrates and analogue. It has been demonstrated that the frequency of the bending mode for the heme propionate is sensitive to the hydrogen-bonding interaction with the protein environment (*38*, *39*) and that the disruption of the hydrogen-bonding network lowers the bending frequency of the heme propionate by ~10 cm^{-1} (*38*). On the basis of these studies, the Raman lines at 377 and 371 cm^{-1} can be assigned to the bending modes of heme propionate with and without hydrogen-bonding interaction with the protein environment, respectively. We, therefore, propose that substrate binding might generate a hydrogen-bonding network involving the heme propionate group.

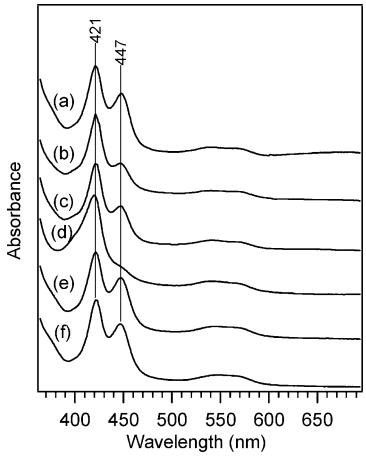

FIGURE 4: Optical absorption spectra of ferrous−CO P450arom in the absence (a) and presence of AD (b), Test (c), 19-OH-AD (d), 19-aldo-AD (e), and 19-nor-AD (f).

It should be stressed that all substrates and analogue gave essentially the same spectral changes in the low-frequency region of RR spectra. While the UV/vis absorption and high-frequency region of RR spectrum for 19-OH-AD-bound P450arom showed that the coordination structure and the spin state were different from other substrate- and analogue-bound P450arom, its binding effect on the low-frequency Raman spectrum was similar to those in other substrate- and analogue-bound P450arom. This observation suggests that the binding mode for the steroid ring would be conserved among the substrates and analogue.

Resonance Raman Spectra of Ferrous−CO P450arom. Our current results on ferric P450arom indicate that the effects of substrate binding on the structural environment of the heme in P450arom are similar among the substrates and analogue. Each substrate-bound P450arom, however, exhibits different reactivity to the molecular oxygen and different sensitivity to the inhibition by CO (*40*), allowing us to speculate that the heme environment of P450arom would depend on the substrates. To confirm this, we measured the absorption spectra for the ferrous−CO form of P450arom and tried to detect the CO-associated vibrations that are sensitive to the distal environment and the electronic property of the proximal ligand (*29*−*31*).

Figure 4 illustrates the optical absorption spectra for the ferrous−CO forms of P450arom in the absence and presence

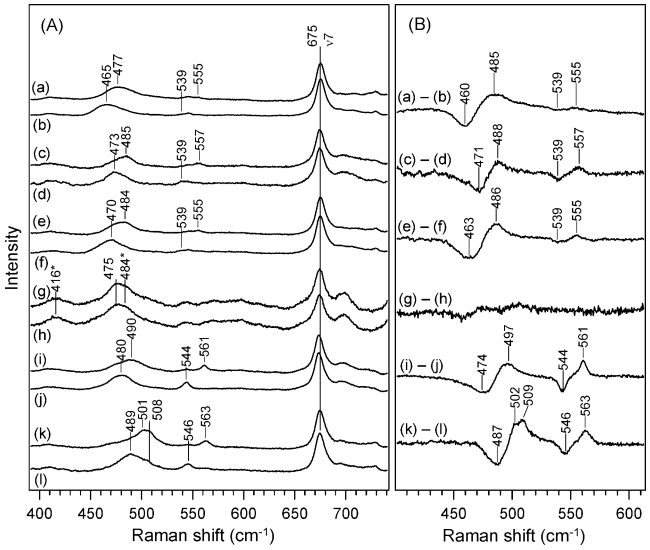

FIGURE 5: Low-frequency region of resonance Raman spectra of ferrous−CO P450arom with 441.6 nm excitation. Panel A represents the spectra obtained from $^{12}C^{16}O$-bound P450arom in the absence of substrate (a) and in the presence of AD (c), Test (e), 19-OH-AD (g), 19-aldo-AD (i), and 19-nor-AD (k) and from $^{13}C^{18}O$-bound P450arom in the absence of substrate (b) and in the presence of AD (d), Test (f), 19-OH-AD (h), 19-aldo-AD (j), and 19-nor-AD (l). The Raman lines from glycerol in the buffer are denoted by an asterisk in traces g and h. The laser power was 1 mW at the sample point. Panel B represents the difference spectra ($^{12}C^{16}O - {}^{13}C^{18}O$) in the Fe−CO stretching and Fe−C−O bending frequency region.

of substrate. As shown in Figure 4a, the Soret peaks were observed at ∼420 and ∼450 nm in the substrate-free P450arom. The higher absorbance at ∼420 nm than that at ∼450 nm indicates that the inactive P420 form is a major species in the ferrous−CO state. Because the P420 form is not a major species in the ferric state, which was confirmed by the structural transition from 6cLS to 5cHS by the binding of substrate in the current work, it is plausible that the reduction of the heme iron could destabilize the thiolate coordination and increase in the population of the P420 form.

In AD- and Test-bound P450arom (Figure 4b,c), the population of the active P450 species was relatively low as compared with that of the substrate-free form. Interestingly, as shown in Figure 4d, the absorbance at ∼450 nm was observed as a shoulder peak in 19-OH-AD-bound P450arom. Furthermore, the contribution of a 5-coordinated ferrous heme was also detected in 19-OH-AD-bound P450arom, which is evident from the shoulder peak at ∼410 nm. In contrast to AD-, Test-, and 19-OH-AD-bound P450arom, the population of the active P450 species of ferrous−CO P450arom was comparable to that of substrate-free P450arom in the presence of 19-aldo-AD or 19-nor-AD (Figure 4e,f).

Although some fraction of P450arom is easily converted to the inactive P420 species upon reduction and substrates such as AD-, Test-, and 19-OH-AD-bound P450arom still contain the nonligated 5-coordinate ferrous state as shown in Figure 4, it should be noted here that the 441.6 nm line from a He−Cd laser can selectively excite the active form of ferrous−CO P450arom. Figure 5A illustrates the RR spectra for the ferrous−CO form of P450arom excited at 441.6 nm. In substrate-free P450arom [Figure 5A(a,b)], a broad line centered at 477 cm^{-1} and a weak line at 555 cm^{-1} were assigned to ν_{Fe-CO} and δ_{FeCO}, respectively, on the basis

Table 3: Frequencies (cm^{-1}) of the Iron−Ligand Vibrations for P450arom and Other Thiolate-Ligated Heme Proteins

sample	ν_{Fe-CO}	δ_{FeCO}	$I(\delta_{FeCO})/I(\nu_{Fe-CO})$	ν_{Fe-S}	ref
P450arom	477	555	0.17	nd[a]	this study
+AD	485	557	0.29	349	this study
+Test	484	555	0.29	349	this study
+19-OH-AD	nd[a]	nd[a]	nd[a]	346	this study
+19-aldo-AD	490	561	0.45	344	this study
+19-nor-AD	501	563	0.38	349	this study
P450cam	464	556	nr[b]	nd[a]	*34*
+D-camphor	481	558	nr[b]	351	*34*, *45*
P450 BM3	471	558	nr[b]	nd[a]	*66*
+arachidonic acid	nr[b]	nr[b]	nr[b]	356	*46*
P450scc[c]	476	nr[b]	nr[b]	nr[b]	*42*
+cholesterol	482	nr[b]	nr[b]	nr[b]	*42*
+22(*R*)-OH-cholesterol	479	nr[b]	nr[b]	nr[b]	*42*
TXAS + CTA_2	nr[b]	nr[b]	nr[b]	350	*54*
CPO	485	560	nr[b]	347	*43*, *47*
eNOS + L-Arg	512	567	nr[b]	338	*44*, *48*
iNOS[d]	487	560	nr[b]	nr[b]	*44*
+L-Arg	512	567	nr[b]	nr[b]	*44*
nNOS[e]	491	562	nr[b]	nr[b]	*43*
+L-Arg	503	566	nr[b]	nr[b]	*43*

[a] nd: not determined. [b] nr: not reported. [c] Cytochrome P450 side-chain cleavage. [d] Inducible NOS. [e] Neuronal NOS.

of the difference spectrum obtained from the isotope substitution for CO [Figure 5, (a) − (b)], which is illustrated in Figure 5B.

The addition of substrates and analogue dramatically alters the peak positions and shapes for the Raman lines associated with CO as observed for other P450s (*34*, *41*, *42*) and NOSs (*43*, *44*). The ν_{Fe-CO} line was shifted to 485 (for AD-bound P450arom) and 484 cm^{-1} (for Test-bound P450arom), and the δ_{FeCO} line was intensified by the addition of AD or Test [Figure 5A(c,e)]. On the other hand, in the 19-OH-AD-bound enzyme, neither ν_{Fe-CO} nor δ_{FeCO} lines were detected [Figure 5A(g)]. The isotope difference spectrum clearly shows this [Figure 5B, (g) − (h)]. Because the absorbance of the CO complex of 19-OH-AD-bound P450arom at ∼450 nm was smaller than those of AD- and Test-bound P450arom (Figure 4), we could not detect the CO-associated modes. Therefore, it is ascribed to the low population of the CO complex for 19-OH-AD-bound P450arom.

The binding of 19-aldo-AD or 19-nor-AD induced an upshift of the ν_{Fe-CO} line by more than 10 cm^{-1} with remarkable intensification of the δ_{FeCO} line [Figure 5A(i,k)]. For 19-nor-AD-bound P450arom, two peaks were observed at 501 and 508 cm^{-1} in the ν_{Fe-CO} region [Figure 5A(k)]. Because the Raman line at 508 cm^{-1} was still detected in the $^{13}C^{18}O$ complex as a shoulder peak [Figure 5A(l)], it is likely that the Raman line at 508 cm^{-1} would be attributed to a porphyrin vibration but not to the Fe−CO vibration. The peak positions for ν_{Fe-CO} and δ_{FeCO} for P450arom in the absence and presence of the substrates and analogue are summarized in Table 3 together with those of thiolate-ligated enzymes. We have also tried to detect the ν_{C-O} band expected in the 1900−2000 cm^{-1} region. Unfortunately, we failed to observe the CO stretching modes for P450arom with and without substrates due to the strong fluorescence.

Iron−Axial Ligand Stretching Modes. Because the substrate binding site is in the heme distal site at close proximity

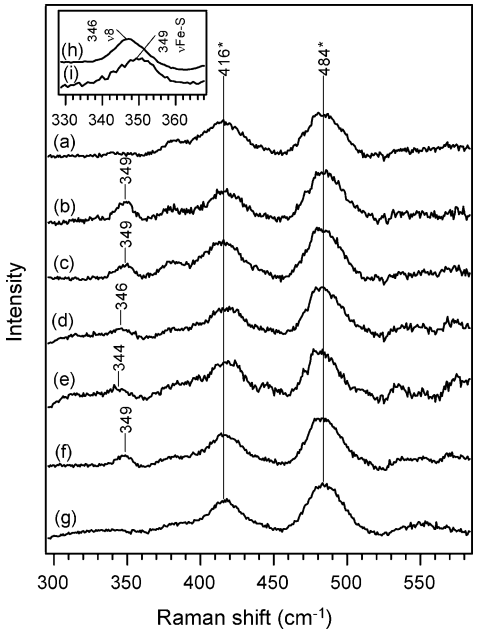

FIGURE 6: Low-frequency region of resonance Raman spectra of ferric P450arom excited at 363.8 nm. Traces shown were obtained from ferric P450arom in the absence of substrate (a) and in the presence of AD (b), Test (c), 19-OH-AD (d), 19-aldo-AD (e), and 19-nor-AD (f) and the buffer used in this measurement (g). The Raman lines from glycerol in the buffer are denoted by an asterisk. The inset is the Fe−S stretching frequency region of the resonance Raman spectra for AD-bound P450arom with 406.7 nm (h) and 363.8 nm (i) excitations. The laser power was 2 mW at the sample point.

to the ligated CO, it is highly plausible that the changes in the distal environment upon the binding of substrates could be the major determinant for a change in ν_{Fe-CO} of P450arom. We, then, attempted to delineate the effects of the substrate binding on the heme proximal site and tried to identify the Fe−S(Cys) stretching mode (ν_{Fe-S}) as a structural marker at the proximal side in P450arom. The ν_{Fe-S} modes in P450s, NOS, and chloroperoxidase (CPO) were reported to be observable only for the ferric 5cHS state excited in the UV region corresponding to the Fe−S charge-transfer band (*45*−*48*). Figure 6 illustrates the low-frequency region of the RR spectra for ferric P450arom in the absence and presence of substrates and analogue with 363.8 nm excitation. The intensities of the Raman lines were greatly decreased upon 363.8 nm excitation, and the RR spectrum for substrate-free P450arom in the low-frequency region (300−550 cm^{-1}) was almost superimposable on that of the buffer (Figure 6a,g). Contrary to this, a new band is present at 349 cm^{-1} for AD-bound ferric P450arom (Figure 6b). This band was not observed by the excitation at 406.7 nm as shown in the inset of Figure 6h although the ν_8 band is present at 346 cm^{-1}. The property of this vibration at 349 cm^{-1} is quite similar to the ν_{Fe-S} vibrations of other P450s and endothelial NOS, which are observed in the range from 338 to 356 cm^{-1} (Table 3) (*45*−*48*). The Raman line at 349 cm^{-1} is, therefore, assigned to the ν_{Fe-S} mode of AD-bound P450arom. The ν_{Fe-S} vibrations in Test- and 19-nor-AD-bound P450arom were also observed at 349 cm^{-1} (Figure 6c,f).

Unexpectedly, the ν_{Fe-S} vibration was downshifted to 346 and 344 cm^{-1} upon addition of 19-OH-AD and 19-aldo-AD, respectively (Figure 6d,e). While the peak position of the ν_{Fe-S} line in 19-OH-AD-bound P450arom coincides with that

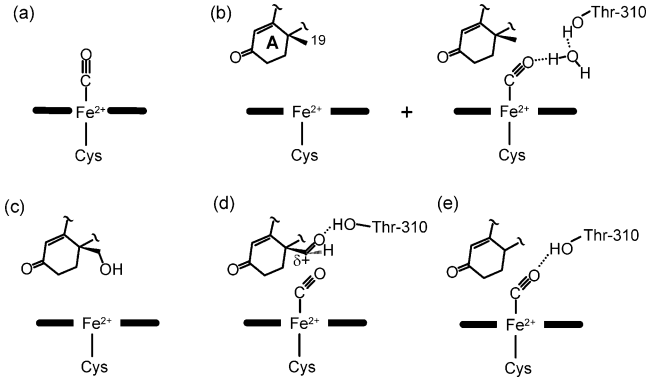

FIGURE 7: Plausible models for the heme active site of the CO complex of P450arom in the absence (a) and presence of AD (Test) (b), 19-OH-AD (c), 19-aldo-AD (d), and 19-nor-AD (e). The dotted lines indicate presumed hydrogen bonds.

of the ν_8 line at 346 cm^{-1}, the ν_8 modes in P450arom in the absence and presence of other substrates were not enhanced with the 363.8 nm excitation. This supports the assignment of the Raman line at 346 cm^{-1} in 19-OH-AD-bound P450arom to the ν_{Fe-S} vibration. The frequencies of ν_{Fe-S} for P450arom in the presence of the substrates are summarized in Table 3. Thus, the substrates for P450arom could modulate not only the heme distal site but also the heme proximal site, even though the substrate binding site is on the heme distal site.

DISCUSSION

In this study, we successfully measured the RR spectra of the ferric and ferrous−CO forms of purified P450arom and found that the CO-associated vibrations and ν_{Fe-S} depend on the specific substrate. These results imply that the binding of substrate would affect both the distal and proximal side of the heme. By using the CO-associated vibrations and ν_{Fe-S} as structural markers at heme distal and proximal sites, respectively, we will deduce the heme environment in P450arom with and without substrates and propose the regulation mechanism for the formation of the alternative reaction intermediates in P450arom catalysis.

Structural Effects of Substrate Binding on the Heme Environments of P450arom. Figure 7 illustrates plausible heme active site structures of ferrous−CO P450arom. In the substrate-free form, the weak intensity of δ_{FeCO} relative to that of ν_{Fe-CO} indicates that the FeCO unit would adopt an essentially linear conformation (Figure 7a) (*31*). In addition, the ν_{Fe-CO} vibration at 477 cm^{-1} is comparable to those of the substrate-free forms of other P450s, suggesting that there are no strong polar interactions between CO and the surrounding residues in substrate-free P450arom.

The fact that the population of the CO adduct in AD-, Test-, and 19-OH-AD-bound P450arom was lower than those of the substrate-free and 19-nor-AD-bound enzyme (Figure 4) may suggest that the C19 groups in AD, Test, and 19-OH-AD can cause a steric hindrance for CO binding (Figure 7b,c). While the population of the CO form was low, the CO-associated modes were observed in AD- and Test-bound P450arom. The intense δ_{FeCO} mode relative to the ν_{Fe-CO} mode [1.7-fold higher in $I(\delta_{FeCO})/I(\nu_{Fe-CO})$ than that of substrate-free P450arom] indicates that the FeCO unit could be distorted by the steric hindrance imposed by AD or Test and would adopt a bent conformation (*31*). With changing

the geometry of the FeCO unit, the environment around CO might be more polar and positive, resulting in the upshift of ν_{Fe-CO} in AD- and Test-bound P450arom (Figure 7b). Because the hydroxyl groups of the conserved Thr and water molecules are observed around the oxygen atom of the FeCO moiety in the crystal structure of the CO complex of P450cam with its substrate (*49*, *50*), the conserved Thr (Thr-310) and/or water molecules might be in close proximity to the CO ligand in AD- and Test-bound P450arom, which induces the upshift of ν_{Fe-CO}. Considering that the hydroxyl group of Thr-310 possibly interacts with the aldehyde group in 19-aldo-AD-bound P450arom (see following discussion) (*24*), we can suggest that the water molecule rather than Thr-310 is present near the CO ligand in the AD- and Test-bound P450arom (Figure 7b).

Contrary to AD-, Test-, and 19-OH-AD-bound P450arom, the population of the ferrous−CO form in 19-aldo-AD-bound P450arom was comparable to those of substrate-free and 19-nor-AD-bound P450arom as seen in Figure 4. This observation raises the possibility that the orientation of the C19 group in 19-aldo-AD-bound P450arom would be different from those of other substrate-bound P450aroms and would not block the CO binding. Graham-Lorence et al. proposed that the conserved Thr (Thr-310) at the heme distal site could be hydrogen-bonded to the oxygen atom of the aldehyde group in 19-aldo-AD to enhance the positive character on the carbonyl carbon and promote the nucleophilic attack of the ferric peroxo species in the third oxidative step (*24*). It is, therefore, likely that the hydrogen-bonding interaction between 19-aldo-AD and Thr-310 could induce the displacement of the C19 group in the 19-aldo-AD-bound P450arom to reduce the steric hindrance for CO binding (Figure 7d). However, similar to AD- and Test-bound P450arom, the $I(\delta_{FeCO})/I(\nu_{Fe-CO})$ value in 19-aldo-AD-bound P450arom [$I(\delta_{FeCO})/I(\nu_{Fe-CO}) = 0.45$] was greater than that of substrate-free P450arom [$I(\delta_{FeCO})/I(\nu_{Fe-CO}) = 0.17$] (Table 3), indicating that the FeCO unit adopts a bent conformation (Figure 7d). It is, therefore, likely that 19-aldo-AD could still be located at close proximity to the CO ligand and that the positive character on the carbonyl carbon of 19C would induce the upshift of ν_{Fe-CO}.

In 19-nor-AD-bound P450arom, the largest upshift of ν_{Fe-CO} indicates that the CO ligand could be in a highly polar environment. Wang et al. reported in the study on inducible NOS that the substrate, L-Arg, binding induces the upshift of ν_{Fe-CO} by 25 cm^{-1} (*44*), which is closely similar to that induced by the binding of 19-nor-AD in P450arom (24 cm^{-1}). The infrared study on the CO complex of inducible NOS by Jung et al. provided the evidence for the hydrogen-bonding interaction between ligated CO and L-Arg (*51*). We, therefore, suggest that the CO ligand could directly interact with the surrounding amino acid residue such as Thr-310 through the hydrogen-bonding interaction in 19-nor-AD-bound P450arom (Figure 7e). Because the C19 group is absent in contrast to the substrates, we can assume that the hydroxyl group of Thr-310 directly hydrogen-bonds to the CO ligand in 19-nor-AD-bound P450arom. Such hydrogen-bonding interaction would result in the bent conformation of the FeCO unit in 19-nor-AD-bound P450arom as depicted in Figure 7e, which could enhance the intensity of δ_{FeCO}. This view is consistent to the presence of the hydrogen bond between 19-aldo-AD and Thr-310.

Besides the changes in the distal environment, the lower electron donation from the axial thiolate might also contribute to the upshift of ν_{Fe-CO} in 19-aldo-AD-bound P450arom. While ν_{Fe-S} was observed at the ferric state, the ν_{Fe-S} mode would correlate with the ν_{Fe-CO} mode in some cases (*43*, *52*, *53*). Indeed, the ν_{Fe-CO} and ν_{C-O} correlation plot showed that the electron donation from thiolate to the heme iron in NOSs ($\nu_{Fe-S} = 338$ cm^{-1} for L-Arg-bound eNOS) is lower than those of P450s ($\nu_{Fe-S} = \sim 350$ cm^{-1}) (*45*, *46*, *48*, *52*, *54*) and that the ν_{Fe-CO} modes in NOSs were observed at the frequency region higher than those of P450s. On the other hand, a recent systematic study on P450 BM3 by Chen et al. reported that the ν_{Fe-S} frequency did not change in the series of mutants whose redox potentials varied over 180 mV (*46*), raising the possibility that the ν_{Fe-S} frequency would not be a reliable indicator of the electron-donating capacity of the thiolate ligand. This is in conflict with our proposal. However, because the redox potential is modulated not only by the electron donation from the axial ligand but also by several factors including the solvent accessibility at the redox cofactor and the redox state-dependent dynamics, the redox potential might not have a correlation with the ν_{Fe-S} mode in P450 BM3. Although further study is required for the clarification of the correlation between the electron-donating property of thiolate and the ν_{Fe-S} mode, the lower electron donation from the axial thiolate in addition to the more positive distal environment might result in the relatively higher ν_{Fe-CO} in 19-aldo-AD-bound P450arom than those of AD- and Test-bound P450aroms.

Implication for the Molecular Mechanism of P450arom Catalysis. The current data indicated that the distal and proximal environments were dependent on the substrates, providing new aspects of the P450arom-catalyzed reaction. One is that the substrate-dependent structural changes in the heme distal site possibly modulate the formation of the alternative reaction intermediates. While, contrary to the FeCO moiety, the FeOO moiety of the oxygen adduct generally adopts a bent conformation (*55*−*59*), the environment of the O_2 ligand also might be expected to depend on the substrates. The geometry difference in the FeOO moiety among different substrates might enable the enzyme to form the alternative reaction intermediates.

The view that the substrate-dependent structural rearrangement in the heme distal site regulates the formation of the alternative reaction intermediates can be consistent with the "Thr switch" model which was originally proposed by Graham-Lorence et al. (*24*). In the Thr switch model, 19-aldo-AD would induce the displacement of distal Thr-310 through the hydrogen-bonding interaction for the formation of ferric peroxo species instead of compound I (*24*). On the basis of the Thr switch model and our current results, we propose the heme active site structure of the oxygen complex of P450arom as shown in Figure 8. Because extensive mechanistic studies on P450cam demonstrated that compound I formation requires protonation of the distal oxygen atom in the oxygen complex by the water molecule hydrogen-bonded to the conserved Thr (*56*, *60*, *61*), the O_2 ligand would be hydrogen-bonded to the water molecule in the first and second oxidative steps in P450arom (Figure 8a). On the other hand, the plausible hydrogen-bonding interaction between the aldehyde group in 19-aldo-AD and Thr-310 could induce the displacement of Thr-310 and the water

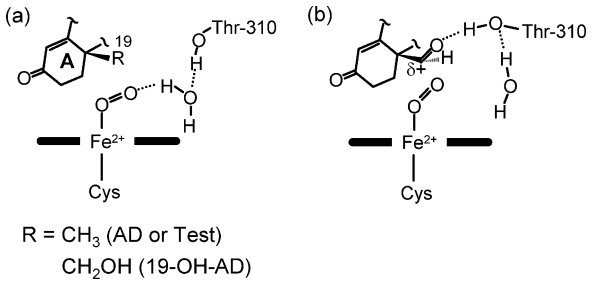

FIGURE 8: Proposed structures of the heme active site of the O_2 complex of P450arom for the first and second oxygen activation reactions (a) and the third oxygen activation reaction (b). The dotted lines indicate presumed hydrogen bonds.

molecule, which could cause the disruption of the hydrogen-bonding interaction between ligated O_2 and the water molecule (Figure 8b). Such location changes in Thr-310 and the water molecule might suppress the protonation of the distal oxygen atom in the ferric peroxo species and eventually inhibit the formation of compound I in the third oxidative step in P450arom.

Another interesting structural aspect of P450arom is that the substrates could regulate the electronic property of the axial thiolate. Because the strong electron donation from the axial thiolate to the heme iron, namely "push effect", has been believed to be one of the key factors controlling the reactivity and stability of compound I (*32*), the reduced electron donation from the axial thiolate to the heme iron in 19-aldo-AD-bound P450arom compared to those of the other substrates could suppress the heterolysis of the O−O bond for the formation of compound I. In other words, the ferric peroxo species would be stabilized by the poor electron donation from the axial thiolate only in the third oxygen activation step of the P450arom catalysis.

The downshift of ν_{Fe-S}, however, was also observed for 19-OH-AD-bound P450arom, suggesting that the reduced axial push effect in 19-aldo-AD-bound P450arom might not be the only factor for the suppression of the formation of compound I. In NOS, while compound I acts as an active species in the first step for the hydroxylation of L-Arg, the electron donation from the axial thiolate is quite low, which is evident from the lower ν_{Fe-S} frequency (ν_{Fe-S} 338 cm^{-1}) than that of P450s (ν_{Fe-S} ~350 cm^{-1}) (*48*). This observation in NOS supports the view that the poor electron donation from the axial thiolate would not be the only factor controlling the formation of the alternative reaction intermediates. Furthermore, a recent systematic study on P450 BM3 suggested that the ν_{Fe-S} mode would not correlate with the electron-donating capacity of the thiolate ligand (*46*). We, therefore, propose that the environmental changes in the heme distal site upon binding of substrates can be essential for regulation of the reactivity and stability of the reaction intermediate and that the substrate-induced change in the electronic property of the axial thiolate might help to stabilize (destabilize) the reaction intermediate in P450arom.

In summary, we have characterized the heme active site structures in P450arom with and without substrates by using RR spectroscopy. From the CO-associated vibrations, we propose that the 19-aldo-AD binding might perturb the proton shuttle machinery responsible for compound I formation, thereby stabilizing the ferric peroxo species in the third oxidative step. In addition, 19-aldo-AD also could lower the electron donation from the axial thiolate, which might suppress compound I formation. It is, therefore, plausible that the substrate can modulate both heme distal and proximal sites to regulate the formation of alternative reaction intermediates in P450arom.

ACKNOWLEDGMENT

We thank Ms. Shiho Kabano (Dojindo Laboratories) for the supply of sodium cholate.

REFERENCES

1. Thompson, E. A., Jr., and Siiteri, P. K. (1974) The involvement of human placental microsomal cytochrome P-450 in aromatization, *J. Biol. Chem. 249*, 5373−5378.
2. Cole, P. A., and Robinson, C. H. (1988) A peroxide model reaction for placental aromatase, *J. Am. Chem. Soc. 110*, 1284−1285.
3. Simpson, E. R., and Davis, S. R. (2001) Minireview: Aromatase and the regulation of estrogen Biosynthesis—some new perspectives, *Endocrinology 142*, 4589−4594.
4. Simpson, E. R., and Dowsett, M. (2002) Aromatase and its inhibitors: Significance for breast cancer therapy, *Recent Prog. Horm. Res. 57*, 317−338.
5. Miller, W. R., and O'Neill, J. (1987) The importance of local synthesis of estrogen within the breast, *Steroids 50*, 537−548.
6. O'Neill, J. S., Elton, R. A., and Miller, W. R. (1988) Aromatase activity in adipose tissue from breast quadrants: A link with tumour site, *Br. Med. J. (Clin. Res. Ed.) 296*, 741−743.
7. Bulun, S. E., Mahendroo, M. S., and Simpson, E. R. (1994) Aromatase gene expression in adipose tissue: Relationship to breast cancer, *J. Steroid Biochem. Mol. Biol. 49*, 319−326.
8. Fishman, J. (1982) Biochemical mechanism of aromatization, *Cancer Res. 42*, 3277−3280.
9. Akhtar, M., Calder, M. R., Corina, D. L., and Wright, J. N. (1982) Mechanistic studies on C-19 demethylation in oestrogen biosynthesis, *Biochem. J. 201*, 569−580.
10. Akhtar, M., Njar, V. C., and Wright, J. N. (1993) Mechanistic studies on aromatase and related C−C bond cleaving P-450 enzymes, *J. Steroid Biochem. Mol. Biol. 44*, 375−387.
11. Miyairi, S., and Fishman, J. (1985) Radiometric analysis of oxidative reactions in aromatization by placental microsomes. Presence of differential isotope effects, *J. Biol. Chem. 260*, 320−325.
12. Numazawa, M., Midzuhashi, K., and Nagaoka, M. (1994) Metabolic aspects of the 1 β-proton and the 19-methyl group of androst-4-ene-3,6,17-trione during aromatization by placental microsomes and inactivation of aromatase, *Biochem. Pharmacol. 47*, 717−726.
13. Korzekwa, K. R., Trager, W. F., Mancewicz, J., and Osawa, Y. (1993) Studies on the mechanism of aromatase and other cytochrome P450 mediated deformylation reactions, *J. Steroid Biochem. Mol. Biol. 44*, 367−373.
14. Hackett, J. C., Brueggemeier, R. W., and Hadad, C. M. (2005) The final catalytic step of cytochrome p450 aromatase: A density functional theory study, *J. Am. Chem. Soc. 127*, 5224−5237.
15. Fischer, R. T., Trzaskos, J. M., Magolda, R. L., Ko, S. S., Brosz, C. S., and Larsen, B. (1991) Lanosterol 14 α-methyl demethylase. Isolation and characterization of the third metabolically generated oxidative demethylation intermediate, *J. Biol. Chem. 266*, 6124−6132.
16. Akhtar, M., Corina, D., Miller, S., Shyadehi, A. Z., and Wright, J. N. (1994) Mechanism of the acyl-carbon cleavage and related reactions catalyzed by multifunctional P-450s: Studies on cytochrome P-450(17)α, *Biochemistry 33*, 4410−4418.
17. Mak, A. Y., and Swinney, D. C. (1992) 17-*O*-Acetyltestosterone formation from progesterone in microsomes from pig testes: Evidence for the Baeyer−Villiger rearrangement in androgen formation catalyzed by CYP17, *J. Am. Chem. Soc. 114*, 8309−8310.
18. Swinney, D. C., and Mak, A. Y. (1994) Androgen formation by cytochrome P450 CYP17. Solvent isotope effect and pL studies suggest a role for protons in the regulation of oxene versus peroxide chemistry, *Biochemistry 33*, 2185−2190.
19. Marletta, M. A. (1993) Nitric oxide synthase structure and mechanism, *J. Biol. Chem. 268*, 12231−12234.

20. Groves, J. T., and Wang, C. C. (2000) Nitric oxide synthase: Models and mechanisms, *Curr. Opin. Chem. Biol. 4*, 687−695.
21. Vaz, A. D., Pernecky, S. J., Raner, G. M., and Coon, M. J. (1996) Peroxo-iron and oxenoid-iron species as alternative oxygenating agents in cytochrome P450-catalyzed reactions: Switching by threonine-302 to alanine mutagenesis of cytochrome P450 2B4, *Proc. Natl. Acad. Sci. U.S.A. 93*, 4644−4648.
22. Vaz, A. D., McGinnity, D. F., and Coon, M. J. (1998) Epoxidation of olefins by cytochrome P450: Evidence from site-specific mutagenesis for hydroperoxo-iron as an electrophilic oxidant, *Proc. Natl. Acad. Sci. U.S.A. 95*, 3555−3560.
23. Jin, S., Bryson, T. A., and Dawson, J. H. (2004) Hydroperoxoferric heme intermediate as a second electrophilic oxidant in cytochrome P450-catalyzed reactions, *J. Biol. Inorg. Chem. 9*, 644−653.
24. Graham-Lorence, S., Amarneh, B., White, R. E., Peterson, J. A., and Simpson, E. R. (1995) A three-dimensional model of aromatase cytochrome P450, *Protein Sci. 4*, 1065−1080.
25. Kagawa, N., Hori, H., Waterman, M. R., and Yoshioka, S. (2004) Characterization of stable human aromatase expressed in *E. coli*, *Steroids 69*, 235−243.
26. Kagawa, N., Cao, Q., and Kusano, K. (2003) Expression of human aromatase (CYP19) in *Escherichia* coli by N-terminal replacement and induction of cold stress response, *Steroids 68*, 205−209.
27. Abe, M., Kitagawa, T., and Kyogoku, Y. (1978) Resonance Raman-spectra of octaethylporphyrinato-NiII and meso-deuterated and ^{15}N-subsutituted derivatives. II. A normal coordinate analysis, *J. Chem. Phys. 69*, 4526−4534.
28. Spiro, T. G., and Li, X.-Y. (1988) Resonance Raman spectroscopy of metalloporphyrin, in *Biological Applications of Raman Spectroscopy* (Spiro, T. G., Ed.) pp 1−37, John Wiley and Sons, New York.
29. Spiro, T. G., and Wasbotten, I. H. (2005) CO as a vibrational probe of heme protein active sites, *J. Inorg. Biochem. 99*, 34−44.
30. Yu, N. T., and Kerr, E. A. (1988) Vibrational modes of coordinated CO, CN^-, O_2 and NO, in *Biological Applications of Raman Spectroscopy* (Spiro, T. G., Ed.) John Wiley and Sons, New York.
31. Ray, G. B., Li, X.-Y., Ibers, J. A., Sessler, J. L., and Spiro, T. G. (1994) How far can proteins bend the FeCO unit? Distal polar and steric effects in heme proteins and models, *J. Am. Chem. Soc. 116*, 162−176.
32. Dawson, J. H. (1988) Probing structure−function relations in heme-containing oxygenases and peroxidases, *Science 240*, 433−439.
33. Modugno, F., Weissfeld, J. L., Trump, D. L., Zmuda, J. M., Shea, P., Cauley, J. A., and Ferrell, R. E. (2001) Allelic variants of aromatase and the androgen and estrogen receptors: Toward a multigenic model of prostate cancer risk, *Clin. Cancer Res. 7*, 3092−3096.
34. Wells, A. V., Li, P., Champion, P. M., Martinis, S. A., and Sligar, S. G. (1992) Resonance Raman investigations of *Escherichia coli*-expressed *Pseudomonas putida* cytochrome P450 and P420, *Biochemistry 31*, 4384−4393.
35. Li, H., Narasimhulu, S., Havran, L. M., Winkler, J. D., and Poulos, T. L. (1995) Crystal structure of cytochrome P450cam complexed with its catalytic product, 5-*exo*-hydroxycamphor, *J. Am. Chem. Soc. 117*, 6297−6299.
36. Hu, S., Morris, I. K., Singh, J. P., Smith, K. M., and Spiro, T. G. (1993) Complete assignment of cytoshrome *c* resonance Raman spectra via enzymatic reconstitution with isotopically labeled hemes, *J. Am. Chem. Soc. 115*, 12446−12458.
37. Hu, S., Smith, K. M., and Spiro, T. G. (1996) Assignment of protoheme resonance Raman spectrum by heme labeling in myoglobin, *J. Am. Chem. Soc. 118*, 12638−12646.
38. Peterson, E. S., Friedman, J. M., Chien, E. Y., and Sligar, S. G. (1998) Functional implications of the proximal hydrogen-bonding network in myoglobin: A resonance Raman and kinetic study of Leu89, Ser92, His97, and F-helix swap mutants, *Biochemistry 37*, 12301−12319.
39. Hildebrand, D. P., Burk, D. L., Maurus, R., Ferrer, J. C., Brayer, G. D., and Mauk, A. G. (1995) The proximal ligand variant His93Tyr of horse heart myoglobin, *Biochemistry 34*, 1997−2005.
40. Meigs, R. A., and Ryan, K. J. (1971) Enzymatic aromatization of steroids. I. Effects of oxygen and carbon monoxide on the intermediate steps of estrogen biosynthesis, *J. Biol. Chem. 246*, 83−87.
41. Uno, T., Nishimura, Y., Makino, R., Iizuka, T., Ishimura, Y., and Tsuboi, M. (1985) The resonance Raman frequencies of the Fe−CO stretching and bending modes in the CO complex of cytochrome P-450cam, *J. Biol. Chem. 260*, 2023−2026.
42. Tsubaki, M., Yoshikawa, S., Ichikawa, Y., and Yu, N. T. (1992) Effects of cholesterol side-chain groups and adrenodoxin binding on the vibrational modes of carbon monoxide bound to cytochrome P-450scc: Implications of the productive and nonproductive substrate bindings, *Biochemistry 31*, 8991−8999.
43. Wang, J., Stuehr, D. J., and Rousseau, D. L. (1997) Interactions between substrate analogues and heme ligands in nitric oxide synthase, *Biochemistry 36*, 4595−4606.
44. Fan, B., Wang, J., Stuehr, D. J., and Rousseau, D. L. (1997) NO synthase isozymes have distinct substrate binding sites, *Biochemistry 36*, 12660−12665.
45. Champion, P. M., Stallard, B. R., Wagner, G. C., and Gunsalus, I. C. (1982) Resonance Raman detection of an iron−sulfur bond in cytochrome P450cam, *J. Am. Chem. Soc. 104*, 5469−5472.
46. Chen, Z., Ost, T. W., and Schelvis, J. P. (2004) Phe393 mutants of cytochrome P450 BM3 with modified heme redox potentials have altered heme vinyl and propionate conformations, *Biochemistry 43*, 1798−1808.
47. Bangcharoenpaurpong, O., Champion, P. M., Hall, K. S., and Hager, L. P. (1986) Resonance Raman studies of isotopically labeled chloroperoxidase, *Biochemistry 25*, 2374−2378.
48. Schelvis, J. P., Berka, V., Babcock, G. T., and Tsai, A. L. (2002) Resonance Raman detection of the Fe−S bond in endothelial nitric oxide synthase, *Biochemistry 41*, 5695−5701.
49. Raag, R., and Poulos, T. L. (1989) Crystal structure of the carbon monoxide-substrate-cytochrome P-450CAM ternary complex, *Biochemistry 28*, 7586−7592.
50. Nagano, S., Tosha, T., Ishimori, K., Morishima, I., and Poulos, T. L. (2004) Crystal structure of the cytochrome P450cam mutant that exhibits the same structural perturbations induced by putidaredoxin binding, *J. Biol. Chem. 279*, 42844−42849.
51. Jung, C., Stuehr, D. J., and Ghosh, D. K. (2000) FT-Infrared spectroscopic studies of the iron ligand CO stretch mode of iNOS oxygenase domain: Effect of arginine and tetrahydrobiopterin, *Biochemistry 39*, 10163−10171.
52. Rousseau, D. L., Li, D., Couture, M., and Yeh, S. R. (2005) Ligand-protein interactions in nitric oxide synthase, *J. Inorg. Biochem. 99*, 306−323.
53. Santolini, J., Roman, M., Stuehr, D. J., and Mattioli, T. A. (2006) Resonance Raman study of *Bacillus subtilis* NO synthase-like protein: Similarities and differences with mammalian NO synthases, *Biochemistry 45*, 1480−1489.
54. Chen, Z., Wang, L. H., and Schelvis, J. P. (2003) Resonance Raman investigation of the interaction of thromboxane synthase with substrate analogues, *Biochemistry 42*, 2542−2551.
55. Berglund, G. I., Carlsson, G. H., Smith, A. T., Szoke, H., Henriksen, A., and Hajdu, J. (2002) The catalytic pathway of horseradish peroxidase at high resolution, *Nature 417*, 463−468.
56. Schlichting, I., Berendzen, J., Chu, K., Stock, A. M., Maves, S. A., Benson, D. E., Sweet, R. M., Ringe, D., Petsko, G. A., and Sligar, S. G. (2000) The catalytic pathway of cytochrome p450cam at atomic resolution, *Science 287*, 1615−1622.
57. Vojtechovsky, J., Chu, K., Berendzen, J., Sweet, R. M., and Schlichting, I. (1999) Crystal structures of myoglobin-ligand complexes at near-atomic resolution, *Biophys. J. 77*, 2153−2174.
58. Condon, P. J., and Royer, W. E., Jr. (1994) Crystal structure of oxygenated Scapharca dimeric hemoglobin at 1.7-Å resolution, *J. Biol. Chem. 269*, 25259−25267.
59. Unno, M., Matsui, T., Chu, G. C., Couture, M., Yoshida, T., Rousseau, D. L., Olson, J. S., and Ikeda-Saito, M. (2004) Crystal structure of the dioxygen-bound heme oxygenase from *Corynebacterium diphtheriae*: Implications for heme oxygenase function, *J. Biol. Chem. 279*, 21055−21061.
60. Nagano, S., and Poulos, T. L. (2005) Crystallographic study on the dioxygen complex of wild-type and mutant cytochrome P450cam: Implications for the dioxygen activation mechanism, *J. Biol. Chem. 280*, 31659−31663.
61. Kimata, Y., Shimada, H., Hirose, T., and Ishimura, Y. (1995) Role of Thr-252 in cytochrome P450cam: A study with unnatural amino acid mutagenesis, *Biochem. Biophys. Res. Commun. 208*, 96−102.
62. Matsuura, K., Yoshioka, S., Tosha, T., Hori, H., Ishimori, K., Kitagawa, T., Morishima, I., Kagawa, N., and Waterman, M. R. (2005) Structural diversities of active site in clinical azole-bound forms between sterol 14α-demethylases (CYP51s) from human and *Mycobacterium tuberculosis*, *J. Biol. Chem. 280*, 9088−9096.

63. Bangcharoenpaurpong, O., Champion, P. M., Martinis, S. A., and Sligar, G. S. (1987) Investigations of the resonance Raman excitation profiles of cytochrome-P450cam, *J. Chem. Phys. 87*, 4273−4284.

64. Remba, R. D., Champion, P. M., Fitchen, D. B., Chiang, R., and Hager, L. P. (1979) Resonance Raman investigations of chloroperoxidase, horseradish peroxidase, and cytochrome *c* using Soret band laser excitation, *Biochemistry 18*, 2280−2290.

65. Champion, P. M., Gunsalus, I. C., and Wagner, G. C. (1978) Resonance Raman investigations of cytochrome P450cam from *Pseudomonas putida*, *J. Am. Chem. Soc. 100*, 3743−3751.

66. Deng, T. J., Proniewicz, L. M., Kincaid, J. R., Yeom, H., Macdonald, I. D., and Sligar, S. G. (1999) Resonance Raman studies of cytochrome P450 BM3 and its complexes with exogenous ligands, *Biochemistry 38*, 13699−13706.

BI060094A